

## INFORMATION TO USERS

This manuscript has been reproduced from the microfilm master. UMI films the text directly from the original or copy submitted. Thus, some thesis and dissertation copies are in typewriter face, while others may be from any type of computer printer.

**The quality of this reproduction is dependent upon the quality of the copy submitted.** Broken or indistinct print, colored or poor quality illustrations and photographs, print bleedthrough, substandard margins, and improper alignment can adversely affect reproduction.

In the unlikely event that the author did not send UMI a complete manuscript and there are missing pages, these will be noted. Also, if unauthorized copyright material had to be removed, a note will indicate the deletion.

Oversize materials (e.g., maps, drawings, charts) are reproduced by sectioning the original, beginning at the upper left-hand corner and continuing from left to right in equal sections with small overlaps.

Photographs included in the original manuscript have been reproduced xerographically in this copy. Higher quality 6" x 9" black and white photographic prints are available for any photographs or illustrations appearing in this copy for an additional charge. Contact UMI directly to order.

ProQuest Information and Learning  
300 North Zeeb Road, Ann Arbor, MI 48106-1346 USA  
800-521-0600

UMI<sup>®</sup>

PREVIEW

**SYNTHESIS AND CHARACTERIZATION OF STABLE IRON(IV), TIN(IV) AND  
RUTHENIUM(IV) THIATRANE COMPLEXES**

by

**Kerry A. Fusie-Clark**

**A DISSERTATION**

**Presented to the Faculty of**

**The Graduate College at the University of Nebraska**

**In Partial Fulfillment of Requirements**

**For the Degree of Doctor of Philosophy**

**Major: Chemistry**

**Under the Supervision of Professor T. Adrian George**

**Lincoln, Nebraska**

**July, 2001**

UMI Number: 3016312

UMI<sup>®</sup>

---

UMI Microform 3016312

Copyright 2001 by Bell & Howell Information and Learning Company.

All rights reserved. This microform edition is protected against  
unauthorized copying under Title 17, United States Code.

---

Bell & Howell Information and Learning Company  
300 North Zeeb Road  
P.O. Box 1346  
Ann Arbor, MI 48106-1346

DISSERTATION TITLE

Synthesis and Characterization of Stable Iron(IV), Tin(IV) and

Ruthenium(IV) Thiatrane Complexes

BY

Ms. Kerry A. Fusie-Clark

SUPERVISORY COMMITTEE:

APPROVED

DATE

T. Adrian George  
Signature  
Dr. T. Adrian George

July 12, 2001

George Sturgeon  
Typed Name  
Signature  
Dr. George Sturgeon

7/12/01

Victor H Day  
Typed Name  
Signature  
Dr. Victor Day

7/12/01

Peter Dowben  
Typed Name  
Signature  
Dr. Peter Dowben

7-12-01

John Stezowski  
Typed Name  
Signature  
Dr. John Stezowski

07/12/01

Signature

Typed Name



GRADUATE COLLEGE  
UNIVERSITY OF NEBRASKA

# SYNTHESIS AND CHARACTERIZATION OF STABLE IRON(IV), TIN(IV) AND RUTHENIUM(IV) THIATRANE COMPLEXES

Kerry A. Fusie-Clark, Ph.D.

University of Nebraska, 2001

Advisor: T. Adrian George

Iron(IV) is proposed to be a key oxidation state in many metalloenzymes that catalyze the selective oxidation of hydrocarbons and related compounds using oxygen. This work reports the designed synthesis of stable, diamagnetic, trigonal bipyramidal, iron(IV) thiatrane complexes starting from either iron(II) or iron(III). For example, the reaction of the tris-thiolate ligand,  $P(C_6H_3-3-SiMe_3-2-S)_3$ ,  $(PS_3)^{TMS}$ , (generated in situ from the  $H_3PS_3^{TMS}$  proligand and  $Et_3N$ ) with  $FeCl_2$  under a nitrogen atmosphere produced an emerald green solution which contained  $[Fe^{II}(PS_3)^{TMS}]^-$ . Laboratory workup of this compound produced an intensely purpled-colored complex,  $ClFe^{IV}(PS_3)^{TMS}$ , which was the first diamagnetic iron(IV) complex and the first trigonal bipyramidal, iron(IV) thiatrane complex to be structurally characterized.

Utilizing this general procedure and a variety of tris-thiolate ligands, this dissertation focuses on the synthesis of complexes of the type  $XM^{IV}(PS_3)$ . Eight additional iron(IV) and the isostructural tin(IV) and ruthenium(IV) complexes with formulas  $XFe(PS_3)^{TMS}$  where  $(PS_3)^{TMS} = P(C_6H_3-3-Me_3Si-2-S)_3$  and  $X = Br, I$ ,

CN,  $\text{PhSn}(\text{PS}_3)^{\text{TMS}}$ ,  $\text{PhSn}(\text{PS}_3)^{\text{Me}}$  where  $(\text{PS}_3)^{\text{Me}} = \text{P}(\text{C}_6\text{H}_3\text{-5-Me-2-S})_3$ ,  $\text{PhSn}(\text{PS}_3)$  where  $(\text{PS}_3) = \text{P}(\text{C}_6\text{H}_4\text{-2-S})_3$ ,  $\text{ClRu}(\text{PS}_3)^{\text{TMS}}$  and  $\text{ClRu}(\text{PS}_3)$  have been synthesized. The mechanistic details for the formation of these stable complexes, the identification of metal and nonmetal-containing reaction coproducts and physical and chemical properties of these substances have been pursued.

Five of these complexes,  $\text{BrFe}(\text{PS}_3)^{\text{TMS}}$ ,  $\text{IFe}(\text{PS}_3)^{\text{TMS}}$ ,  $\text{PhSn}(\text{PS}_3)^{\text{TMS}}$ ,  $\text{PhSn}(\text{PS}_3)^{\text{Me}}$  and  $\text{PhSn}(\text{PS}_3)$  have been studied crystallographically.  $\text{PhSn}(\text{PS}_3)^{\text{TMS}}$  can be easily converted to either  $\text{ClFe}(\text{PS}_3)^{\text{TMS}}$  or  $\text{ClRu}(\text{PS}_3)^{\text{TMS}}$  via transmetalation reactions using  $\text{FeCl}_3$ ,  $\text{FeCl}_2$ ,  $(\text{Et}_4\text{N})_2[\text{Fe}_2\text{OCl}_6]$  and  $\text{RuCl}_2(\text{DMSO})_4$ . These reactions gave insight into the lability of the fifth coordination site (halogen, cyanide or phenyl) in the trigonal bipyramidal complexes as well as the reactivity of the metal centers. The chemical reactivity of  $\text{ClFe}(\text{PS}_3)^{\text{TMS}}$  has been explored by using this iron(IV) complex as a reagent in the attempted formation of six-coordinate  $(\text{Et}_2\text{NCS}_2)\text{Fe}(\text{PS}_3)^{\text{TMS}}$ .

Developing this chemistry and characterizing the resulting complexes provided the foundation needed to prepare a new group of functional and structural models for a wide range of metalloenzymes.

## **Table of Contents**

List of Figures	x
List of Tables	xv
List of Equations	xvii
List of Charts	xviii
Abbreviations	xix
Acknowledgements	xxiii
Chapter 1      Project History	1
Chapter 2      Synthesis and Characterization of	7
Tripodal, Tris-thiolate, Phosphine Ligands	
Introduction	7
Experimental	9
Preparation of Compounds	11
Preparation of 2-Me <sub>3</sub> SiC <sub>6</sub> H <sub>4</sub> SH	11
Preparation of H <sub>3</sub> PS <sub>3</sub> <sup>TMS</sup>	13
Preparation of H <sub>3</sub> PS <sub>3</sub>	15
Preparation of H <sub>3</sub> PS <sub>3</sub> <sup>Me</sup>	17
Preparation of (PS <sub>3</sub> )P	18
Results	19
H <sub>3</sub> PS <sub>3</sub> <sup>TMS</sup>	19



$\text{H}_3\text{PS}_3$	25
$(\text{OPS}_3)_2$	33
$[(\text{OPS}_3)_2^{\text{TMS}}\text{H}]^+$	34
$(\text{PS}_3)^{\text{TMS}}\text{P}$	35
$(\text{PS}_3)\text{P}$	36
$\text{H}_3\text{PS}_3^{\text{Me}}$	37
Discussion	38
<b>Chapter 3      Synthesis and Characterization of</b>	<b>48</b>
<b>                 Thiastannatranes</b>	
Introduction	48
Experimental	51
Preparation of Compounds	53
Preparation of $\text{PhSn}(\text{PS}_3)^{\text{TMS}}$	53
Preparation of $\text{PhSn}(\text{PS}_3)$	54
Preparation of $\text{PhSn}(\text{PS}_3)^{\text{Me}}$	56
Preparation of $n\text{-BuSn}(\text{PS}_3)$	57
Preparation of $\text{CH}_3\text{Sn}(\text{PS}_3)$	58
Preparation of $\text{ClRu}(\text{PS}_3)^{\text{TMS}}$	59
Preparation of $\text{ClRu}(\text{PS}_3)$	60
Preparation of $\text{ClFe}(\text{PS}_3)^{\text{TMS}}$	61
Attempted Preparation of $\text{ClFe}(\text{PS}_3)$	63
Results	64

$\text{PhSn(PS}_3\text{)}^{\text{TMS}}$	64
$\text{PhSn(PS}_3\text{)}$	83
$\text{PhSn(PS}_3\text{)}^{\text{Me}}$	91
$n\text{-BuSn(PS}_3\text{)}$	96
$\text{CH}_3\text{Sn(PS}_3\text{)}$	99
$\text{ClRu(PS}_3\text{)}^{\text{TMS}}$	100
$\text{ClRu(PS}_3\text{)}$	101
$\text{ClFe(PS}_3\text{)}^{\text{TMS}}$	102
$\text{ClFe(PS}_3\text{)}$	103
Discussion	104
<b>Chapter 4      Synthesis and Characterization of</b>	<b>126</b>
<b>                 Thiaferratrane</b>	
Introduction	126
Experimental	132
Preparation of Compounds	133
Preparation of $\text{ClFe(PS}_3\text{)}^{\text{TMS}}$	133
Preparation of $\text{BrFe(PS}_3\text{)}^{\text{TMS}}$	139
Preparation of $\text{IFe(PS}_3\text{)}^{\text{TMS}}$	141
Attempted preparation of $\text{FFe(PS}_3\text{)}^{\text{TMS}}$	143
Preparation of $(\text{Et}_2\text{CNS}_2)\text{Fe(PS}_3\text{)}^{\text{TMS}}$	150
Preparation of $(\text{CN})\text{Fe(PS}_3\text{)}^{\text{TMS}}$	152
Preparation of $\text{Fe}_2(\text{PS}_3)$	155

Preparation of $\text{Fe}_2(\text{PS}_3)^{\text{TMS}}$	156
Attempted preparation of $\text{ClFe}(\text{PS}_3)$	157
Attempted preparation of $\text{BrFe}(\text{PS}_3)$	161
Attempted preparation of $(\text{CN})\text{Fe}(\text{PS}_3)$	162
Preparation of $[\text{Et}_3\text{NH}][(\text{CO})\text{Fe}^{\text{II}}(\text{PS}_3)]$	163
Results	163
$\text{ClFe}(\text{PS}_3)^{\text{TMS}}$	163
$\text{BrFe}(\text{PS}_3)^{\text{TMS}}$	173
$\text{IFe}(\text{PS}_3)^{\text{TMS}}$	173
$\text{FFe}(\text{PS}_3)^{\text{TMS}}$	182
$(\text{CN})\text{Fe}(\text{PS}_3)^{\text{TMS}}$	183
$[(\text{CN})\text{Fe}_2(\text{PS}_3)_2^{\text{TMS}}][\text{PF}_6]$	188
$(\text{Et}_2\text{CNS}_2)\text{Fe}(\text{PS}_3)^{\text{TMS}}$	189
$\text{Fe}_2(\text{PS}_3)$	190
$\text{Fe}_2(\text{PS}_3)^{\text{TMS}}$	190
$\text{XFe}(\text{PS}_3)$ where $\text{X} = \text{Cl}, \text{Br}, \text{CN}$	193
$[\text{Et}_3\text{NH}][(\text{CO})\text{Fe}^{\text{II}}(\text{PS}_3)]$	194
Discussion	195
Chapter 5      Synthesis and Characterization of	214
Thiaruthenatranes	
Introduction	214
Experimental	216

Preparation of Compounds	218
Preparation of $\text{ClRu}(\text{PS}_3)^{\text{TMS}}$	218
Preparation of $\text{ClRu}(\text{PS}_3)$	221
Results	224
$\text{ClRu}(\text{PS}_3)^{\text{TMS}}$	224
$\text{ClRu}(\text{PS}_3)$	230
Discussion	235
Chapter 6      Appendix	242
Appendix A: Additional Figures	242
Appendix B: Publication Reprints	253
Appendix C: Crystal Structure Factors	258

## List of Figures

### Chapter 1

Figure 1.1	FeS <sub>3</sub> geometry within FeMoco.	1
Figure 1.2	Tripodal, tris-thiolato PS <sub>3</sub> ligand.	2
Figure 1.3	Structure of ClFe(PS <sub>3</sub> ) <sup>TMS</sup> .	3

### Chapter 2

Figure 2.1	HMQC 2-D NMR spectrum for H <sub>3</sub> PS <sub>3</sub> <sup>TMS</sup> .	22
Figure 2.2	HMBC 2-D NMR spectrum for H <sub>3</sub> PS <sub>3</sub> <sup>TMS</sup> .	23
Figure 2.3	Atom labeling scheme for H <sub>3</sub> PS <sub>3</sub> <sup>TMS</sup> .	24
Figure 2.4	2-D COSY NMR spectrum for H <sub>3</sub> PS <sub>3</sub> .	27
Figure 2.5	<sup>31</sup> P decoupled <sup>1</sup> H NMR spectrum for H <sub>3</sub> PS <sub>3</sub> .	28
Figure 2.6	HMQC 2-D NMR spectrum for H <sub>3</sub> PS <sub>3</sub> .	30
Figure 2.7	HMBC 2-D NMR spectrum for H <sub>3</sub> PS <sub>3</sub> .	31
Figure 2.8	Atom labeling scheme for H <sub>3</sub> PS <sub>3</sub> .	32
Figure 2.9	Ball and stick model of (OPS <sub>3</sub> ) <sub>2</sub> .	34
Figure 2.10	Ball and stick model for [(OPS <sub>3</sub> ) <sub>2</sub> <sup>TMS</sup> H] <sup>+</sup> .	35
Figure 2.11	Structure of (PS <sub>3</sub> ) <sup>TMS</sup> P.	36
Figure 2.12	Plot of chemical shift resonance versus aromatic carbon atom for H <sub>3</sub> PS <sub>3</sub> <sup>TMS</sup> and H <sub>3</sub> PS <sub>3</sub> .	42

### Chapter 3

Figure 3.1	Examples of pentacoordinate tin structures.	49
Figure 3.2	Reported azastannatranes.	49

Figure 3.3	Transmetalation reactions utilizing azastannatranes.	50
Figure 3.4	Representative tricyclic, phenyl stannatranes.	50
Figure 3.5	ORTEP plot of $\text{PhSn}(\text{PS}_3)^{\text{TMS}}$ .	66
Figure 3.6	Ball and stick model of $\text{PhSn}(\text{PS}_3)^{\text{TMS}}$ compared to Figure 3.8.	68
Figure 3.7	Crystallographic packing plot for $\text{PhSn}(\text{PS}_3)^{\text{TMS}}$ .	68
Figure 3.8	Comparison of Spartan geometry optimization structure (colored) to the actual X-ray structure (gray).	69
Figure 3.9	Atom labeling scheme for $\text{PhSn}(\text{PS}_3)^{\text{TMS}}$ .	70
Figure 3.10	HMQC 2-D NMR spectrum for $\text{PhSn}(\text{PS}_3)^{\text{TMS}}$ .	75
Figure 3.11	HMBC 2-D NMR spectrum for $\text{PhSn}(\text{PS}_3)^{\text{TMS}}$ .	76
Figure 3.12	$^{31}\text{P}$ decoupled $^1\text{H}$ NMR spectrum for $\text{PhSn}(\text{PS}_3)^{\text{TMS}}$ in $\text{CD}_2\text{Cl}_2$ .	77
Figure 3.13	$^{29}\text{Si}$ solution spectrum for $\text{PhSn}(\text{PS}_3)^{\text{TMS}}$ .	80
Figure 3.14	$^{29}\text{Si}$ solid state NMR spectrum for $\text{PhSn}(\text{PS}_3)^{\text{TMS}}$ .	81
Figure 3.15	TMS peak in the $^{13}\text{C}$ solid state NMR spectrum of $\text{PhSn}(\text{PS}_3)^{\text{TMS}}$ .	82
Figure 3.16	Aromatic region of the $^{13}\text{C}$ solid state NMR spectrum of $\text{PhSn}(\text{PS}_3)^{\text{TMS}}$ .	83
Figure 3.17	ORTEP plot of $\text{PhSn}(\text{PS}_3)$ .	85
Figure 3.18	Ball and stick model of $\text{PhSn}(\text{PS}_3)$ compared to Figure 3.20.	87
Figure 3.19	Crystallographic packing plot of $\text{PhSn}(\text{PS}_3)$ .	87
Figure 3.20	Comparison of Spartan geometry optimization structure (colored) to the actual X-ray Structure (gray).	88

Figure 3.21	Atom labeling scheme for $\text{PhSn}(\text{PS}_3)$ .	90
Figure 3.22	ORTEP plot of $\text{PhSn}(\text{PS}_3)^{\text{Me}}$ .	92
Figure 3.23	Ball and stick model of $\text{PhSn}(\text{PS}_3)^{\text{Me}}$ compared to Figure 3.25.	94
Figure 3.24	Crystallographic packing plot of $\text{PhSn}(\text{PS}_3)^{\text{Me}}$ .	94
Figure 3.25	Comparison of Spartan geometry optimization structure (colored) to the actual X-ray structure (gray).	95
Figure 3.26	Atom labeling scheme for $n\text{-BuSn}(\text{PS}_3)$ .	98
Figure 3.27	Possible phenyl-plane orientations relative to the $\text{S}_3$ plane.	108
Figure 3.28	Apical phenyl cap orientations for $\text{PhSn}(\text{PS}_3)^{\text{TMS}}$ , $\text{PhSn}(\text{PS}_3)^{\text{Me}}$ and $\text{PhSn}(\text{PS}_3)$ .	109
Figure 3.29	Plot of chemical shift versus aromatic carbon atom for $\text{PhSn}(\text{PS}_3)^{\text{TMS}}$ , $\text{PhSn}(\text{PS}_3)$ and $n\text{-BuSn}(\text{PS}_3)$ .	120

## Chapter 4

Figure 4.1	Structures of $[\text{Ni}(\text{PS}_3)_2]^{2-}$ and $[\text{Ni}(\text{PS}_3)_2]^-$ . The aromatic ligand rings are represented by curved lines for clarity.	130
Figure 4.2	Ball and stick model of the $\text{Fe}_2(\text{PS}_3)^{\text{TMS}}$ dimer. The TMS groups and H atoms have been removed for clarity.	131
Figure 4.3	ORTEP plot of $\text{ClFe}(\text{PS}_3)^{\text{TMS}}$ .	166
Figure 4.4	Crystallographic packing plot of $\text{ClFe}(\text{PS}_3)^{\text{TMS}}$ .	168
Figure 4.5	HMQC 2-D NMR spectrum for $\text{ClFe}(\text{PS}_3)^{\text{TMS}}$ .	170
Figure 4.6	HMBC 2-D NMR spectrum for $\text{ClFe}(\text{PS}_3)^{\text{TMS}}$ .	171
Figure 4.7	Atom labeling scheme for $\text{ClFe}(\text{PS}_3)^{\text{TMS}}$ .	172

Figure 4.8	ORTEP plot of $\text{BrFe}(\text{PS}_3)^{\text{TMS}}$ .	174
Figure 4.9	Crystallographic packing plot of $\text{BrFe}(\text{PS}_3)^{\text{TMS}}$ .	176
Figure 4.10	Low temperature (100 K) ball and stick model of $\text{BrFe}(\text{PS}_3)^{\text{TMS}}$ .	177
Figure 4.11	Atom labeling scheme for $\text{BrFe}(\text{PS}_3)^{\text{TMS}}$ .	178
Figure 4.12	ORTEP plot of $\text{IFe}(\text{PS}_3)^{\text{TMS}}$ .	179
Figure 4.13	Crystallographic packing plot of $\text{IFe}(\text{PS}_3)^{\text{TMS}}$ .	180
Figure 4.14	Atom labeling scheme for $\text{IFe}(\text{PS}_3)^{\text{TMS}}$ .	181
Figure 4.15	Atom labeling scheme for $(\text{CN})\text{Fe}(\text{PS}_3)^{\text{TMS}}$ .	187
Figure 4.16	Structure of $[(\text{CN})\text{Fe}_2(\text{PS}_3)_2]^{\text{TMS}+}$ .	188
Figure 4.17	Ball and stick model of $\text{Fe}_2(\text{PS}_3)_2^{\text{TMS}}$ .	192
Figure 4.18	Plot of chemical shift versus aromatic carbon atom for $\text{ClFe}(\text{PS}_3)^{\text{TMS}}$ and the pro-ligand.	204
Figure 4.19	Stability of $\text{XFe}^{\text{IV}}(\text{PS}_3)^{\text{TMS}}$ in various solvent systems.	205
Figure 4.20	Molecular orbital diagram for $\text{XFe}^{\text{IV}}(\text{PS}_3)^{\text{TMS}}$ .	206
Figure 4.21	Formation of a six-coordinate $\text{Fe}(\text{IV})$ complex.	207

## Chapter 5

Figure 5.1	Molecular orbital diagram of $\text{Ru}^{\text{IV}}(\text{PS}_3)$ versus $\text{Fe}^{\text{IV}}(\text{PS}_3)$ . The orbital diagram is not drawn to scale.	215
Figure 5.2	A. The ligand present in $[\text{Ru}^{\text{II}}(\text{P}_2\text{S}_6)]$ . B. The resulting compound.	216
Figure 5.3	HMQC 2-D NMR spectrum for $\text{ClRu}(\text{PS}_3)^{\text{TMS}}$ .	226
Figure 5.4	HMBC 2-D NMR spectrum for $\text{ClRu}(\text{PS}_3)^{\text{TMS}}$ .	228
Figure 5.5	Atom labeling scheme for $\text{ClRu}(\text{PS}_3)^{\text{TMS}}$ .	229



Figure 5.6	2-D COSY NMR spectrum for ClRu(PS <sub>3</sub> ).	232
Figure 5.7	<sup>31</sup> P decoupled <sup>1</sup> H NMR spectrum for ClRu(PS <sub>3</sub> ).	233
Figure 5.8	Atom labeling scheme for ClRu(PS <sub>3</sub> ).	234
Figure 5.9	Plot of chemical shift versus aromatic carbon atom for ClRu(PS <sub>3</sub> ) <sup>TMS</sup> , ClRu(PS <sub>3</sub> ) and their pro-ligands.	239

## Chapter 6

Figure 6.1	Structure of FeMo-cofactor of Nitrogenase.	243
Figure 6.2	<sup>31</sup> P NMR resonance of (PS <sub>3</sub> ) <sup>TMS</sup> P.	244
Figure 6.3	<sup>31</sup> P NMR resonance of PhSn(PS <sub>3</sub> ).	245
Figure 6.4	<sup>1</sup> H NMR spectrum of ClFe(PS <sub>3</sub> ) <sup>TMS</sup> .	246
Figure 6.5	<sup>31</sup> P NMR resonance of IFe(PS <sub>3</sub> ) <sup>TMS</sup> . Reported resonances of ClFe(PS <sub>3</sub> ) <sup>TMS</sup> and BrFe(PS <sub>3</sub> ) <sup>TMS</sup> .	247
Figure 6.6	<sup>31</sup> P NMR resonance for ClRu(PS <sub>3</sub> ). Reported resonance for ClRu(PS <sub>3</sub> ) <sup>TMS</sup> .	248
Figure 6.7	Blue arrows: Observed <sup>13</sup> C- <sup>31</sup> P coupling for ClRu(PS <sub>3</sub> ) <sup>TMS</sup> . Green arrows: Observed <sup>1</sup> H and <sup>13</sup> C bond correlations via an HMBC 2-D NMR experiment.	249
Figure 6.8	Blue arrows: Observed <sup>13</sup> C- <sup>31</sup> P coupling for ClRu(PS <sub>3</sub> ). Red arrows: Observed <sup>1</sup> H bond connectivities via a 2-D COSY NMR experiment.	250
Figure 6.9	Representative compound colors.	251
Figure 6.10	Plot of chemical shift versus aromatic carbon for six compounds and their respective proligands.	252

## List of Tables

### Chapter 2

Table 2.1	Examples of tripodal, tetradentate pro-ligands.	8
Table 2.2	$^{13}\text{C}$ and $^1\text{H}$ NMR resonance assignments for $\text{H}_3\text{PS}_3^{\text{TMS}}$ .	24
Table 2.3	$^{13}\text{C}$ and $^1\text{H}$ NMR resonance assignments for $\text{H}_3\text{PS}_3$ .	33
Table 2.4	Comparison of $^{13}\text{C}$ NMR resonance assignments for $\text{H}_3\text{PS}_3^{\text{TMS}}$ and $\text{H}_3\text{PS}_3$ .	41

### Chapter 3

Table 3.1	Important bond lengths and angles for $\text{PhSn}(\text{PS}_3)^{\text{TMS}}$ .	66
Table 3.2	Spartan's predicted bond angles and bond distances for $\text{PhSn}(\text{PS}_3)^{\text{TMS}}$ .	70
Table 3.3	$^1\text{H}$ NMR data for $\text{PhSn}(\text{PS}_3)^{\text{TMS}}$ at 300 and 500 MHz in $\text{CD}_2\text{Cl}_2$ and $d_8\text{-thf}$ .	71
Table 3.4	$^{13}\text{C}$ NMR resonance assignments for $\text{PhSn}(\text{PS}_3)^{\text{TMS}}$ .	78
Table 3.5	Important bond lengths and angles for $\text{PhSn}(\text{PS}_3)$ .	85
Table 3.6	Spartan's predicted bond angles and bond distances for $\text{PhSn}(\text{PS}_3)$ .	89
Table 3.7	$^{13}\text{C}$ and $^1\text{H}$ NMR resonance assignments for $\text{PhSn}(\text{PS}_3)$ .	90
Table 3.8	Important bond lengths and angles for $\text{PhSn}(\text{PS}_3)^{\text{Me}}$ .	93
Table 3.9	Spartan's predicted bond angles and bond distances for $\text{PhSn}(\text{PS}_3)^{\text{Me}}$ .	96
Table 3.10	$^{13}\text{C}$ and $^1\text{H}$ NMR resonance assignments for $n\text{-BuSn}(\text{PS}_3)$ .	98
Table 3.11	Collection of important bond lengths and angles for $\text{PhSn}(\text{PS}_3)^{\text{TMS}}$ , $\text{PhSn}(\text{PS}_3)$ and $\text{PhSn}(\text{PS}_3)^{\text{Me}}$ .	107

Table 3.12	Comparison of $^{13}\text{C}$ NMR resonance assignments for three tin complexes and their pro-ligands.	119
------------	--	-----

## Chapter 4

Table 4.1	Iron(II) and Iron(III) compounds with thiatrane ligands.	128
Table 4.2	Important bond lengths and angles for $\text{ClFe}(\text{PS}_3)^{\text{TMS}}$	167
Table 4.3	$^{13}\text{C}$ and $^1\text{H}$ NMR resonance assignments for $\text{ClFe}(\text{PS}_3)^{\text{TMS}}$ .	172
Table 4.4	Important bond lengths and angles for $\text{BrFe}(\text{PS}_3)^{\text{TMS}}$ .	175
Table 4.5	$^1\text{H}$ NMR resonance assignments for $\text{BrFe}(\text{PS}_3)^{\text{TMS}}$ .	178
Table 4.6	Important bond lengths and angles for $\text{IFe}(\text{PS}_3)^{\text{TMS}}$ .	180
Table 4.7	$^1\text{H}$ NMR resonance assignments for $\text{IFe}(\text{PS}_3)^{\text{TMS}}$ .	181
Table 4.8	$^1\text{H}$ NMR resonance assignments for $(\text{CN})\text{Fe}(\text{PS}_3)^{\text{TMS}}$ .	187
Table 4.9	$^1\text{H}$ NMR resonance assignments for $[(\text{CN})\text{Fe}(\text{PS}_3)_2]^{\text{TMS}+}$ .	188
Table 4.10	Summary of reactions to form $\text{XFe}^{\text{IV}}(\text{PS}_3)^{\text{TMS}}$ .	197
Table 4.11	Comparison of $^{13}\text{C}$ NMR resonance assignments of $\text{ClFe}(\text{PS}_3)^{\text{TMS}}$ and the pro-ligand.	204

## Chapter 5

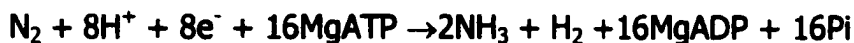
Table 5.1	$^{13}\text{C}$ and $^1\text{H}$ NMR resonance assignments for $\text{ClRu}(\text{PS}_3)^{\text{TMS}}$ .	229
Table 5.2	$^{13}\text{C}$ and $^1\text{H}$ NMR resonance assignments for $\text{ClRu}(\text{PS}_3)$ .	234
Table 5.3	Comparison of $^{13}\text{C}$ NMR resonances for assignments for $\text{ClRu}(\text{PS}_3)^{\text{TMS}}$ , $\text{ClRu}(\text{PS}_3)$ and their pro-ligands.	238

# List of Equations

## Chapter 1

### Equation 1.1

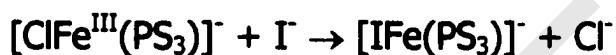
1



## Chapter 4

### Equation 4.1

198



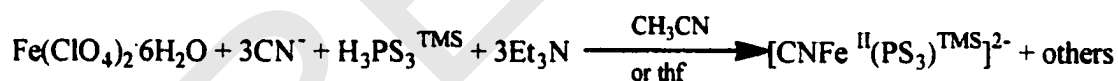
### Equation 4.2

199



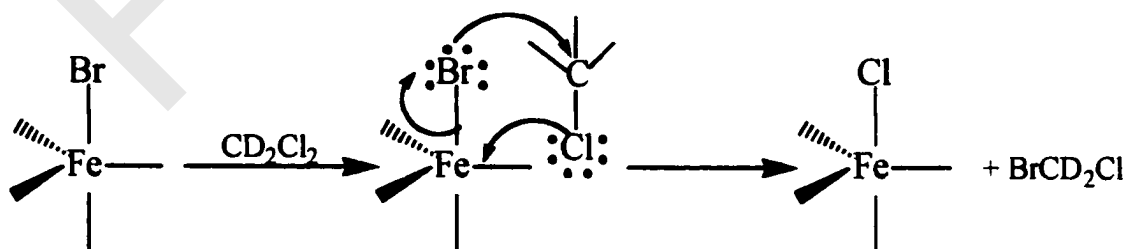
### Equation 4.3

200



### Equation 4.4

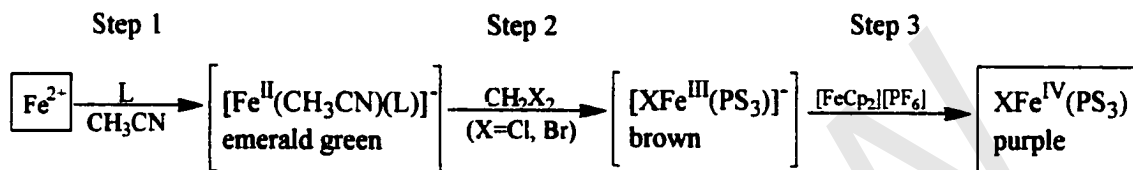
208



## List of Charts

Chart 4.1 Synthetic pathway to  $\text{XFe}^{\text{IV}}(\text{PS}_3)^{\text{TMS}}$ .  $\text{L} = \text{PS}_3^{\text{TMS}}$ 

195

Chart 4.6 Equilibria associated with  $\text{H}_3\text{PS}_3^{\text{TMS}}$ .

209



## List of Abbreviations

1-D	one-dimensional
2-D	two-dimensional
3-NMA matrix	matrix used for FAB-MS
°C	degrees Celsius
δ	delta
η	eta
μ	mu
ν	nu
Å	angstrom
acac	acetylacetonate
ADP	adenosine diphosphate
ATP	adenosine triphosphate
Br	broad
<i>n</i> -Bu	n-butyl
ca.	about or approximately
calcd.	calculated
COSY	Correlated Spectroscopy
CV	cyclic voltammetry
CP/MAS	cross polarization magic angle spinning
Cys	cysteine
d (in parenthesis)	doublet

<b>dd (in parenthesis)</b>	<b>doublet of doublets</b>
<b>ddd (in parenthesis)</b>	<b>doublet of doublet of doublets</b>
<b>dddd (in parenthesis)</b>	<b>doublet of doublet of doublet of doublets</b>
<b>dt (in parenthesis)</b>	<b>doublet of triplets</b>
<b>e<sup>-</sup></b>	<b>electron</b>
<b>ε M<sup>-1</sup>cm<sup>-1</sup></b>	<b>epsilon, per molarity per centimeter</b>
<b>Et</b>	<b>ethyl</b>
<b>FAB-MS</b>	<b>fast atom bombardment ionization mass spectrometry</b>
<b>[FeCp<sub>2</sub>][PF<sub>6</sub>]</b>	<b>ferrocenium hexafluorophosphate</b>
<b>FTIR</b>	<b>fourier transform infrared spectroscopy</b>
<b>g</b>	<b>gram(s)</b>
<b>h</b>	<b>hour(s)</b>
<b>Heme</b>	<b>porphyrin-type ligand in biological systems</b>
<b>His</b>	<b>histidine</b>
<b>HMBC</b>	<b>Heteronuclear Multiple Bond Correlation</b>
<b>HMQC</b>	<b>Heteronuclear Multiple Quantum Coherence</b>
<b>HOMO</b>	<b>highest occupied molecular orbital</b>
<b>Hz</b>	<b>Hertz</b>
<b>J</b>	<b>coupling constant</b>
<b>K</b>	<b>Kelvin</b>
<b>L</b>	<b>Liter</b>

$\lambda_{\text{max}}$	lambda maximum
LUMO	lowest occupied molecular orbital
m (in parenthesis)	multiplet
M	molarity
$M^+$	parent ion (mass spectrometry)
m/z	mass to charge ratio
Me	methyl
MHz	megahertz
mL	milliliter
mm	millimeter
MMO	methane monooxygenase
mmol	millimole
nm	nanometer
NMR	nuclear magnetic resonance
<i>O</i>	ortho
<i>P</i>	para
P-450	used to name a specific cytochrome
Ph	phenyl
Pi	inorganic phosphate
ppm	parts per million
pr <sup>i</sup>	isopropyl
s	second(s)